

Comparing the Calculated Fermi Level Splitting with the Open-Circuit Voltage in Various Perovskite Cells

Guo, Dengyang; Caselli, Valentina M.; Hutter, Eline M.; Savenije, Tom J.

DOI

[10.1021/acsenergylett.9b00431](https://doi.org/10.1021/acsenergylett.9b00431)

Publication date

2019

Document Version

Final published version

Published in

ACS Energy Letters

Citation (APA)

Guo, D., Caselli, V. M., Hutter, E. M., & Savenije, T. J. (2019). Comparing the Calculated Fermi Level Splitting with the Open-Circuit Voltage in Various Perovskite Cells. *ACS Energy Letters*, 4(4), 855-860. <https://doi.org/10.1021/acsenergylett.9b00431>

Important note

To cite this publication, please use the final published version (if applicable). Please check the document version above.

Copyright

Other than for strictly personal use, it is not permitted to download, forward or distribute the text or part of it, without the consent of the author(s) and/or copyright holder(s), unless the work is under an open content license such as Creative Commons.

Takedown policy

Please contact us and provide details if you believe this document breaches copyrights. We will remove access to the work immediately and investigate your claim.

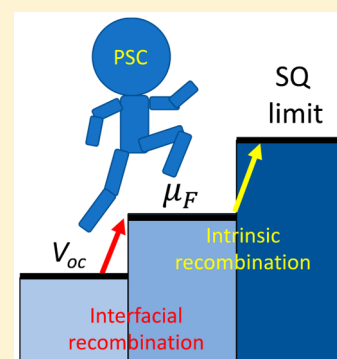
Comparing the Calculated Fermi Level Splitting with the Open-Circuit Voltage in Various Perovskite Cells

Dengyang Guo, Valentina M. Caselli, Eline M. Hutter,[‡] and Tom J. Savenije^{*†}

Department of Chemical Engineering, Delft University of Technology, 2629 HZ Delft, The Netherlands

Supporting Information

ABSTRACT: While the power conversion efficiency of metal halide perovskite (MHP) solar cells has increased enormously, the open-circuit voltage, V_{oc} , is still below the conceivable limit. Here, we derive the Fermi level splitting, μ_F , for various types of noncontacted MHPs, which sets a limit for their achievable V_{oc} using rate constants and mobilities obtained from time-resolved photoconductivity measurements. Interestingly, we find that for vacuum-evaporated MAPbI₃ and K⁺-doped (MA,FA,Cs)Pb(I/Br)₃, the μ_F/e values are close to the reported V_{oc} values. This implies that for an improvement of the V_{oc} , charge carrier recombination within the bare perovskite has to be reduced. On the other hand, for MHPs with Cs⁺ and/or Rb⁺ addition, the experimental V_{oc} is still below μ_F/e , suggesting that higher voltages are feasible by optimizing the transport layers. The presented approach will help to select which techniques and transport layers are beneficial to improve the efficiency of MHP solar cells.



Since their first introduction in 2009,¹ perovskite solar cells (PSCs) have shown an unprecedented rise in energy conversion efficiency, surpassing that of CIGS and approaching the value of crystalline silicon solar cells.² Different optimization approaches, including bandgap utilization,^{3,4} light management,^{5,6} interface engineering,^{7–9} and transport material optimization,^{10–12} have been used to improve the efficiency. Subsequently, the open-circuit voltage, V_{oc} , of PSCs has increased from 0.61¹ to over 1.2 V.^{13–16} However, this value is still below the V_{oc} determined by the bandgap and thermal radiation or so-called entropy losses (1.33 V for MAPbI₃).^{17–19} Hence, understanding the factors governing the V_{oc} and developing methodologies to improve this are essential to exploit the full potential of metal halide perovskites (MHPs). Because optimizing PSCs is labor-intensive, determination of the upper limit of the V_{oc} on the basis of the characteristics of a bare perovskite semiconductor layer is extremely useful.

qV_{oc} is the quasi-Fermi level splitting, μ_F under illumination at open circuit and is defined by²⁰

$$\mu_F = \frac{kT}{q} \ln \frac{(n_0 + \Delta n)(p_0 + \Delta p)}{n_i^2} \quad (1)$$

where $\frac{kT}{q}$ is the thermal energy, n_i is the intrinsic carrier concentration, n_0 and p_0 are thermal equilibrium concentrations of electrons and holes, respectively, and Δn and Δp are the concentrations of photoexcited excess electrons and holes, respectively. From quasi-steady-state photoconductance data

measured by making use of a coil, the effective lifetime of charges in a semiconductor layer can be extracted.²¹ In case the semiconductor properties are known including the charge carrier mobilities, the excess charge carrier densities under AM1.5 can then be calculated, allowing one to come to a value for the Fermi level splitting. We are not aware of any report using this technique for predicting the V_{oc} in perovskite cells, most likely due to the fact that the mobilities vary with composition, morphology, and post-treatment.²¹

An alternative way to quantify μ_F is using photoluminescence (PL), by either fitting the absolute intensity PL spectrum including subgap tail states²² or using the absolute PL quantum yield.^{23–25} However, these methods require knowledge of the PL output coupling and reabsorption features of the MHP in order to calculate the internal PL quantum efficiency. Another approach to come to μ_F is probing the charge carrier dynamics by time-resolved measurements like time-resolved microwave photoconductance (TRMC), optical pump–THz probe spectroscopy (THz), or transient absorption spectroscopy (TAS). In this work, we first present a method how to derive the μ_F under AM1.5 using the rate constants found by fitting time-resolved photoconductance measurements on a spin-coated MAPbI₃ film. In the second part, we apply this approach on previously published TRMC data.^{26–28} Interestingly, we find that for vacuum-

Received: February 25, 2019

Accepted: March 12, 2019

Published: March 12, 2019

evaporated MAPbI₃ layers and for (MA,FA,Cs)Pb(I/Br)₃ doped with K⁺, the calculated μ_F is very close to the reported V_{oc} values. This implies that for an improvement of V_{oc} the charge carrier recombination within the native MHP has to be reduced. Additionally, we observe that the addition of Cs⁺ and/or Rb⁺ to (MA,FA)Pb(I/Br)₃ or light soaking in humid air of MAPbI₃ leads to an increase of both the calculated μ_F and of the observed V_{oc} . However, for these cells, the maximum attainable V_{oc} has not been reached yet. This means that the V_{oc} of these solar cells could be further improved by optimizing the interface with the transport layers. Comparing the calculated μ_F with the V_{oc} helps to select which deposition techniques, additives, postproduction treatments, and transport layers are beneficial to improve the efficiency of MHP solar cells.

In the first part of this Letter, a method to calculate μ_F under continuous illumination with the rate constants describing the charge decay kinetics is presented. To this end, we recorded TRMC traces of MAPbI₃ using a nanosecond pulsed laser at 500 nm while varying the incident intensity over 4 orders of magnitude, shown in Figure 1a. We make use of our kinetic

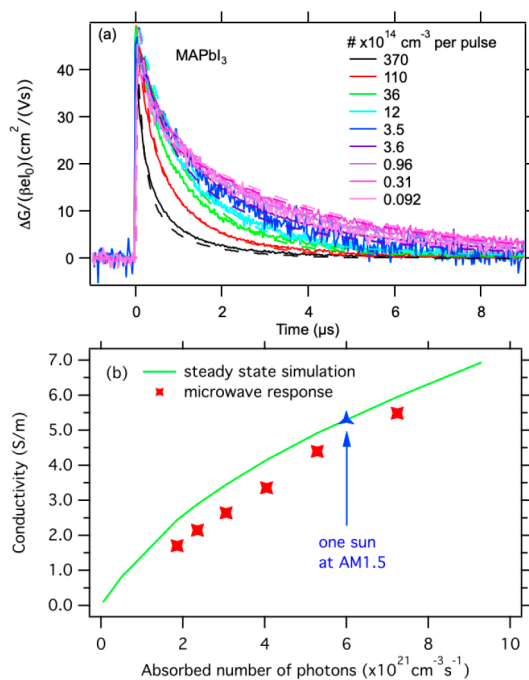
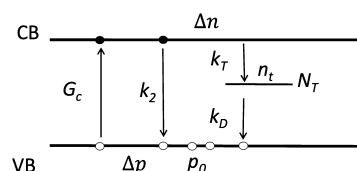


Figure 1. (a) TRMC traces (solid) along with the fits (dashed) of the spin-coated MAPbI₃ thin film. The excitation density per laser pulse is presented by the number of absorbed photons divided by the thickness of the sample. (b) The red markers denote the conductivities obtained from the microwave signal induced by continuous illumination using a white light LED. The green line is the photoconductivity calculated using the charge carrier concentrations found by integration of eqs 2–4 as a function of G_c . The blue arrow corresponds to a G_c identical to the number of absorbed photons using AM1.5.

model reported in 2015, which has been successfully applied to a range of MHP layers.^{28–31} Scheme 1 depicts all of the processes included in the model, in which n_t is the concentration of trapped electrons, p_0 the concentration of background holes, and N_T the density of available deep traps; k_2 , k_T , and k_D are the rate constants representing band-to-band

Scheme 1. Kinetic Model Describing the Charge Carrier Dynamics in Perovskites



recombination, trapping, and trap depopulation, respectively, while G_c represents the optical excitation.

$$\frac{d\Delta n}{dt} = G_c - k_2\Delta n(\Delta p + p_0) - k_T\Delta n(N_T - n_t) \quad (2)$$

$$\frac{d\Delta p}{dt} = G_c - k_2\Delta n(\Delta p + p_0) - k_D n_t(\Delta p + p_0) \quad (3)$$

$$\frac{dn_t}{dt} = k_T\Delta n(N_T - n_t) - k_D n_t(\Delta p + p_0) \quad (4)$$

To obtain values for all kinetic parameters, we solved the coupled differential eqs 2–4 numerically with the same set of parameters except for the generation term, which equals the intensity of the laser pulses. From the resulting time-dependent Δn and Δp , we can determine the time-dependent photoconductance, ΔG , by

$$\Delta G = e(\mu_e \Delta n + \mu_p \Delta p)\beta L \quad (5)$$

where μ_e and μ_p are the mobilities of electrons and holes, respectively. β is the geometrical constant and L the layer thickness. As shown in Figure 1a, the fits match the experimental TRMC traces very well. Note that below a certain excitation density the traces start to overlap, which indicates that the recombination turns from higher order to first order. From this threshold, starting at densities around 4×10^{14} cm⁻³ per pulse, we can accurately ascertain N_T (see Figure S1a,b).

Figure 1a shows that we can use our model shown in Scheme 1 to extract dynamic parameters and to calculate Δn , Δp , and n_t as a function of time. In case all of the essential processes are captured by our kinetic model, it should be possible to switch from pulsed excitation to continuous excitation. Hence, we calculated Δn , Δp , and n_t using eqs 2–4, with the previously obtained set of dynamics parameters but replacing the pulsed G_c by continuous excitation. In Figure S2a,b the time-dependent concentrations are shown using intensities comparable to 1 and 100% of AM1.5 reaching constant values within 20 μ s.

To verify these calculated values for Δn and Δp , we compared the photoconductivity, $\Delta\sigma$, derived from the calculated charge carrier concentrations with $\Delta\sigma$ measured under continuous excitation. In Figure 1b, the red markers denote $\Delta\sigma$ as a function of the absorbed number of photons generated by a white light LED. A more detailed explanation of how we extract $\Delta\sigma$ from the microwave response is provided in the SI with Figures S3–S5. As shown in Figure 1b, excellent agreement between the calculated and measured $\Delta\sigma$ is observed. This resemblance demonstrates that our kinetic model captures all of the essential photophysical processes within intensities between 1 and 100% of AM1.5 and can be used for predicting the steady-state excess charge carrier concentrations. Hence, we can use our pulsed time-resolved

Table 1. Kinetic Parameters Derived from Analysis of the TRMC Traces, Calculated Excess Concentrations, and μ_F/e Values for Different PSCs

	MAPbI ₃ evaporated ^a	(MA,FA)Pb(I/Br) ₃ spin-coated ^b	(MA,FA)Pb(I/Br) ₃ with RbCs spin-coated ^b	(MA,FA,Cs)Pb(I/Br) ₃ spin-coated ^c	(MA,FA,Cs)Pb(I/Br) ₃ with K spin-coated ^c	MAPbI ₃ spin-coated ^d	MAPbI ₃ spin-coated, light soaking ^d
k_2 (10^{-10} cm ³ s ⁻¹)	50	6	3	40	20	2.6	0.76
N_T (10^{13} cm ⁻³)	30	250	80	30	30	6	5.5
Δn (10^{14} cm ⁻³)	3.1	5.8	24	5.5	9	41	78
Δp (10^{14} cm ⁻³)	5.5	17	28	6.8	11	42	78
n_i (10^{13} cm ⁻³)	24	11	41	13	18	6.0	5.5
μ_F/e (V)	1.15	1.18	1.23	1.17	1.16	1.26	1.29
second-order ratio η_2 (%)	62	23	67	82	83	96	97

^aEvaporated MAPbI₃; data from ref 28. ^bSpin-coated mixed perovskite with and without rubidium and cesium; data from ref 39. ^cSpin-coated mixed perovskite with and without 10% potassium; data from ref 26. ^dSpin-coated MAPbI₃, treated by light soaking in humid air; data from ref 27.

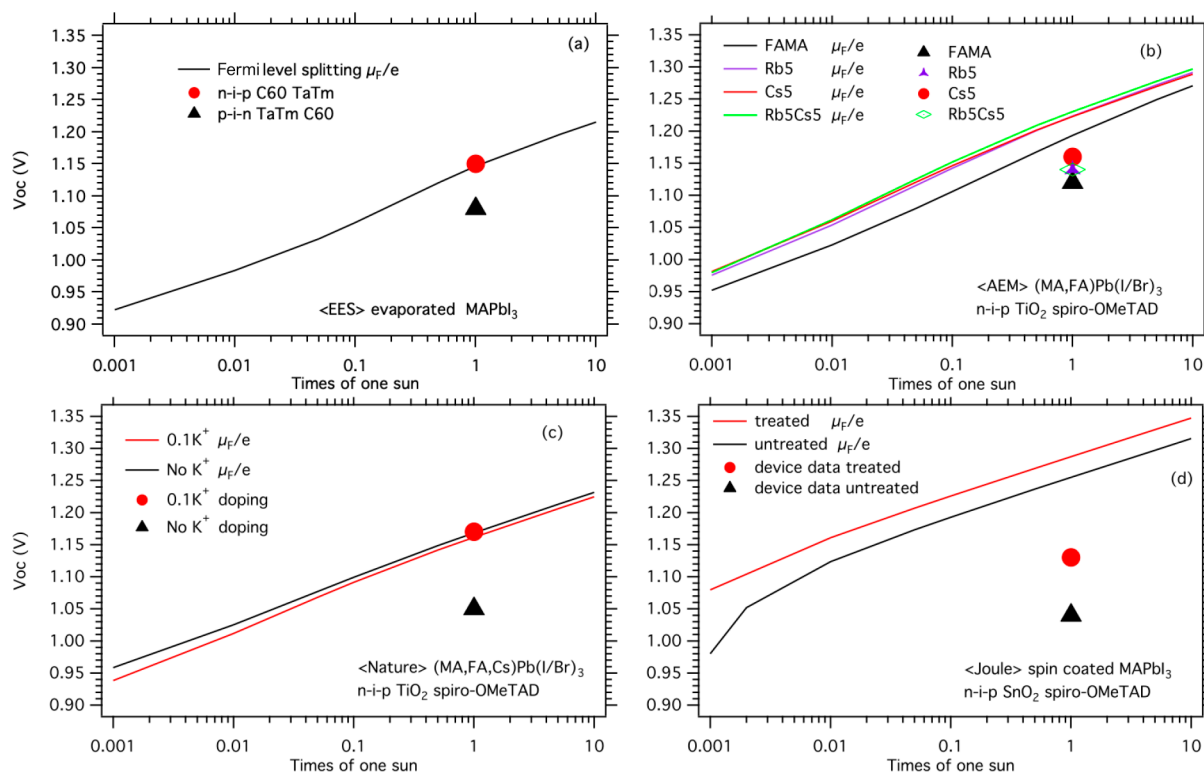


Figure 2. Comparison between the calculated quasi-Fermi level splitting (full lines), μ_F/e , and the corresponding experimental V_{oc} (markers). The data shown in (a–d) are taken from ref 28, 39, 26, and 27, respectively. The deposition method of the MHP layers, device structures, and treatments are given in the annotations.

measurements to evaluate the excess carrier concentration at open circuit in a solar cell.

In the next part, we will process previously published TRMC data in the same way as described above to obtain Δn and Δp under excitation conditions similar to AM1.5, from which we will derive μ_F using eq 1. These μ_F values will then be compared with the V_{oc} values of the corresponding PSCs.^{26–28} These PSCs were made using different precursors and fabrication procedures (spin-coated and evaporated MAPbI₃, (MA,FA,Cs)Pb(I/Br)₃, (MA,FA)Pb(I/Br)₃) and comprise different device structures and transport materials. The effect of additives like K⁺, Cs⁺, and/or Rb⁺ and of postproduction treatments such as light soaking were also investigated. The TRMC traces and fits are shown in Figure S6. Note that these TRMC traces have been recorded on films identical to those used for solar cell fabrication. The key fitting parameters are

listed in Table 1, and the full set of parameters is collected in Table S1. In order to determine μ_F using eq 1, not only are Δn and Δp required but also n_i , n_0 , and p_0 . We calculated n_i of MAPbI₃ to be 12.6×10^4 cm⁻³ from previously published values of the effective masses^{32–38} and a bandgap of 1.58 eV (see eqs S6–S8). For (MA,FA,Cs)Pb(I/Br)₃, we assumed the same effective masses as those of MAPbI₃ but used bandgaps of 1.56 and 1.59 eV for perovskite layers with and without K⁺ doping, respectively. p_0 was obtained by fitting the TRMC traces, and n_0 could be derived by $p_0 n_0 = n_i^2$. However, the values of n_0 and p_0 are negligibly small compared to Δn and Δp , as listed in Table S1. The calculated values of μ_F/e for different excitation intensities along with the experimentally measured V_{oc} values are shown in Figure 2.

Figure 2a shows that, although both solar cells are fabricated using the same evaporated MAPbI₃, the V_{oc} for the n(C60)–i–

p(TaTm) structure is 1.15 V, while for the inverted stack, the V_{oc} is 1.08 V. The former value is actually very close to our calculated value of 1.15 V, which supports the idea that our model can accurately determine μ_F/e and that this value is close to the V_{oc} .^{40,41} This is in agreement with recent studies from Nazeeruddin et al.⁴⁰ and Dänekamp et al.⁴¹ claiming that the Fermi levels of both transport materials sandwiching the MHP have little effect on the V_{oc} of a PSC. Hence, an additional increase of V_{oc} requires improvement of the MAPbI₃, leading to larger excess charge carrier concentrations.²⁸ The lower value for the p–i–n solar cell structure might be related to changes in optoelectronic properties obtained by deposition on different bottom layers.

In Figure 2b, the impact of Cs⁺ and/or Rb⁺ addition to (MA,FA)Pb(I/Br)₃ on μ_F/e and V_{oc} is shown. Cells containing 5% Cs⁺ and/or 5% Rb⁺³⁹ all exhibit a higher V_{oc} following the same trend as our modeled results. Although other groups have found higher V_{oc} values up to 1.19 V,^{42,43} all V_{oc} values are still smaller than the calculated μ_F/e , which implies that deposition of the transport layers results in additional decay pathways and that higher V_{oc} values are feasible by optimizing the transport layers. Interestingly, from our calculations, it is important to note that μ_F/e for (MA,FA)Pb(I/Br)₃ is equal to that of the evaporated MAPbI₃ samples (having the same bandgap), implying that both fabrication methods are capable of producing similar quality MHPs.

For (MA,FA,Cs)Pb(I/Br)₃ with and without K⁺ passivation, the dependencies of μ_F/e with intensity are very similar, while the measured V_{oc} values differ significantly, as shown in Figure 2c. This increase in V_{oc} is attributed to the passivation by K of surface states formed by the deposition of the HTM layer.²⁶ Hence, we suggest that K doping retards the interfacial recombination between the MHP and spiro-OMeTAD. Again, by either optimizing the device structure and/or effectively passivating the interfaces, considerable rise of the V_{oc} can be realized. However, additional increase of V_{oc} requires improvement of the (MA,FA,Cs)Pb(I/Br)₃, leading to higher excess charge carrier concentrations.

An efficient way to improve the μ_F/e of a MAPbI₃ layer is light soaking in humid air.²⁷ As shown in Figure 2d, a μ_F/e value of 1.29 V at 1 sun is observed, which is very close to the theoretical maximum of 1.33 V predicted for MAPbI₃.^{17–19} Despite this great potential, this value has not been realized, although very recent work proved that a V_{oc} of 1.26 V can be obtained by optimizing the transport layers and light soaking.¹⁶

The above presented methodology enables us to evaluate the ratio of second-order recombination over the total decay processes, η_2 , defined by

$$\eta_2 = \frac{R_2}{R_2 + R_T} \quad (6)$$

Here, $R_2 = k_2 \Delta n (\Delta p + p_0)$ and $R_T = k_T \Delta n (N_T - n_t)$, representing the decay of excess electrons by second-order and by trap-mediated processes under steady-state excitation, respectively. Ideally, $\eta_2 = 1$, meaning all excess carriers decay by band-to-band recombination.

As can be observed by the results presented in Table 1, all of the additions or treatments lead to a substantial reduction of k_2 , and the highest η_2 values were obtained by light soaking treatment.²⁷ The small value of N_T is attributed to the improved bulk quality of the MAPbI₃ film mainly by the addition of hypophosphorous acid in combination with PbAc₂ to the perovskite precursor solution.⁴⁴ The light soaking

treatment, which is shown to affect the surface rather than the bulk, only slightly decreases N_T but leads to substantial elongation of the apparent charge carrier lifetime.²⁶ Note that k_2 is the apparent rate constant, as previously discussed by Brenes et al.,²⁶ which means that the value of k_2 might be substantially reduced by, e.g., reabsorption of emitted photons. However, for determination of μ_F/e , the apparent rates are of importance as these also apply in a complete device. The apparent values of k_2 obtained by other techniques, e.g., 8.1×10^{-11} from transient absorption (TA)²¹ or 4.5×10^{-10} from optical pump–THz probe spectroscopy (THz)⁴⁵ are in the same range as our data, which supports the idea that the present approach can also be used for kinetic parameters obtained by these other time-resolved measurements.

In summary, in this paper, we present how to derive μ_F/e from pulsed excitation experiments on bare, noncontacted perovskite films. We show that the obtained values correspond to the measured V_{oc} for a number of MHP solar cells, indicating that decay processes occurring within the perovskite layer are limiting the V_{oc} for those cells, rather than interfacial recombination processes. From our modeling, we conclude that the addition of Cs⁺ and Rb⁺ and even more effectively light soaking in air of MHPs lead to a substantial increase of μ_F/e . Although these additions or treatments have resulted in improved V_{oc} values, these methods bear the promise that higher voltages are still feasible by improving the transport layers and preventing recombination at the interface with these contact layers. This works helps to select which steps can help to improve the efficiency of MHP solar cells.

■ ASSOCIATED CONTENT

Supporting Information

The Supporting Information is available free of charge on the ACS Publications website at DOI: 10.1021/acsenergylett.9b00431.

TRMC response conversion and LED output calibration (PDF)

■ AUTHOR INFORMATION

Corresponding Author

*E-mail: T.J.Savenije@tudelft.nl.

ORCID

Eline M. Hutter: 0000-0002-5537-6545

Tom J. Savenije: 0000-0003-1435-9885

Present Address

‡Hybrid Solar Cells, Center for Nanophotonics, AMOLF, Science Park 104, 1098 XG Amsterdam, The Netherlands.

Notes

The authors declare no competing financial interest.

■ ACKNOWLEDGMENTS

D.G. acknowledges the CSC (China Scholarship Council) for funding, File No. 201504910812. E.M.H. was supported by The Netherlands Organization for Scientific Research (NWO) under the Echo Grant Number 712.014.007. Dr. S. Stranks (Cambridge) and Dr. H. Bolink (Valencia) are acknowledged for providing samples.

REFERENCES

- (1) Kojima, A.; Teshima, K.; Shirai, Y.; Miyasaka, T. Organometal Halide Perovskites as Visible-Light Sensitizers for Photovoltaic Cells. *J. Am. Chem. Soc.* **2009**, *131*, 6050–6051.
- (2) National Renewable Energy Laboratory. Research Cell Record Efficiency Chart <https://www.nrel.gov/pv/assets/images/efficiency-chart.png> (accessed Jan 30, 2019).
- (3) Ono, L. K.; Juarez-Perez, E. J.; Qi, Y. Progress on Perovskite Materials and Solar Cells with Mixed Cations and Halide Anions. *ACS Appl. Mater. Interfaces* **2017**, *9*, 30197–30246.
- (4) Jesper Jacobsson, T.; Correa-Baena, J.-P.; Pazoki, M.; Saliba, M.; Schenk, K.; Grätzel, M.; Hagfeldt, A. Exploration of the Compositional Space for Mixed Lead Halogen Perovskites for High Efficiency Solar Cells. *Energy Environ. Sci.* **2016**, *9*, 1706–1724.
- (5) Peer, A.; Biswas, R.; Park, J.-M.; Shinar, R.; Shinar, J. Light Management in Perovskite Solar Cells and Organic LEDs with Microlens Arrays. *Opt. Express* **2017**, *25*, 10704.
- (6) Manzoor, S.; Yu, Z. J.; Ali, A.; Ali, W.; Bush, K. A.; Palmstrom, A. F.; Bent, S. F.; McGehee, M. D.; Holman, Z. C. Improved Light Management in Planar Silicon and Perovskite Solar Cells Using PDMS Scattering Layer. *Sol. Energy Mater. Sol. Cells* **2017**, *173*, 59–65.
- (7) Hou, Y.; Du, X.; Scheiner, S.; McMeekin, D. P.; Wang, Z.; Li, N.; Killian, M. S.; Chen, H.; Richter, M.; Levchuk, I.; et al. A Generic Interface to Reduce the Efficiency-Stability-Cost Gap of Perovskite Solar Cells. *Science* **2017**, *358*, 1192–1197.
- (8) Christians, J. A.; Schulz, P.; Tinkham, J. S.; Schloemer, T. H.; Harvey, S. P.; Tremolet De Villers, B. J.; Sellinger, A.; Berry, J. J.; Luther, J. M. Tailored Interfaces of Unencapsulated Perovskite Solar Cells for > 1,000 h Operational Stability. *Nat. Energy* **2018**, *3*, 68–74.
- (9) Hou, Y.; Scheiner, S.; Tang, X.; Gasparini, N.; Richter, M.; Li, N.; Schweizer, P.; Chen, S.; Chen, H.; Quiroz, C. O. R.; et al. Suppression of Hysteresis Effects in Organohalide Perovskite Solar Cells. *Adv. Mater. Interfaces* **2017**, *4*, 1700007.
- (10) Shin, S. S.; Yeom, E. J.; Yang, W. S.; Hur, S.; Kim, M. G.; Im, J.; Seo, J.; Noh, J. H.; Seok, S. I. Colloidally Prepared La-Doped BaSnO₃ Electrodes for Efficient, Photostable Perovskite Solar Cells. *Science* **2017**, *356*, 167–171.
- (11) Calió, L.; Kazim, S.; Grätzel, M.; Ahmad, S. Hole-Transport Materials for Perovskite Solar Cells. *Angew. Chem., Int. Ed.* **2016**, *55*, 14522–14545.
- (12) Petrus, M. L.; Schutt, K.; Sirtl, M. T.; Hutter, E. M.; Closs, A. C.; Ball, J. M.; Bijleveld, J. C.; Petrozza, A.; Bein, T.; Dingemans, T. J.; et al. New Generation Hole Transporting Materials for Perovskite Solar Cells: Amide-Based Small-Molecules with Nonconjugated Backbones. *Adv. Energy Mater.* **2018**, *8*, 1801605.
- (13) Li, Y.; Ding, B.; Chu, Q. Q.; Yang, G. J.; Wang, M.; Li, C. X.; Li, C. J. Ultra-High Open-Circuit Voltage of Perovskite Solar Cells Induced by Nucleation Thermodynamics on Rough Substrates. *Sci. Rep.* **2017**, *7*, 1–10.
- (14) Saygili, Y.; Turren-Cruz, S. H.; Olthof, S.; Saes, B. W. H.; Pehlivan, I. B.; Saliba, M.; Meerholz, K.; Edvinsson, T.; Zakeeruddin, S. M.; Grätzel, M.; et al. Planar Perovskite Solar Cells with High Open-Circuit Voltage Containing a Supramolecular Iron Complex as Hole Transport Material Dopant. *ChemPhysChem* **2018**, *19*, 1363–1370.
- (15) Anaraki, E. H.; Kermanpur, A.; Steier, L.; Domanski, K.; Matsui, T.; Tress, W.; Saliba, M.; Abate, A.; Grätzel, M.; Hagfeldt, A.; et al. Highly Efficient and Stable Planar Perovskite Solar Cells by Solution-Processed Tin Oxide. *Energy Environ. Sci.* **2016**, *9*, 3128–3134.
- (16) Liu, Z.; Krückemeier, L.; Krogmeier, B.; Klingebiel, B.; Márquez, J. A.; Levchenko, S.; Öz, S.; Mathur, S.; Rau, U.; Unold, T.; et al. Open-Circuit Voltages Exceeding 1.26 V in Planar Methylammonium Lead Iodide Perovskite Solar Cells. *ACS Energy Lett.* **2019**, *4*, 110–117.
- (17) Sha, W. E. I.; Ren, X.; Chen, L.; Choy, W. C. H. The Efficiency Limit of CH₃NH₃PbI₃ Perovskite Solar Cells. *Appl. Phys. Lett.* **2015**, *106*, 221104.
- (18) Tress, W.; Yavari, M.; Domanski, K.; Yadav, P.; Niesen, B.; Correa Baena, J. P.; Hagfeldt, A.; Graetzel, M. Interpretation and Evolution of Open-Circuit Voltage, Recombination, Ideality Factor and Subgap Defect States during Reversible Light-Soaking and Irreversible Degradation of Perovskite Solar Cells. *Energy Environ. Sci.* **2018**, *11*, 151–165.
- (19) Tress, W.; Marinova, N.; Inganäs, O.; Nazeeruddin, M. K.; Zakeeruddin, S. M.; Graetzel, M. Predicting the Open-Circuit Voltage of CH₃NH₃PbI₃ Perovskite Solar Cells Using Electroluminescence and Photovoltaic Quantum Efficiency Spectra: The Role of Radiative and Non-Radiative Recombination. *Adv. Energy Mater.* **2015**, *5*, 1400812.
- (20) Neamen, D. A. *Semiconductor Physics & Devices: Basic Principles*, 4th ed.; McGraw-Hill Education: New York, 2012; pp 10121.
- (21) Sinton, R. A.; Cuevas, A. Contactless Determination of Current-Voltage Characteristics and Minority-Carrier Lifetimes in Semiconductors from Quasi-Steady-State Photoconductance Data. *Appl. Phys. Lett.* **1996**, *69*, 2510–2512.
- (22) Braly, I. L.; Dequillettes, D. W.; Pazos-Outón, L. M.; Burke, S.; Ziffer, M. E.; Ginger, D. S.; Hillhouse, H. W. Hybrid Perovskite Films Approaching the Radiative Limit with over 90% Photoluminescence Quantum Efficiency. *Nat. Photonics* **2018**, *12*, 355–361.
- (23) Kirchartz, T.; Krückemeier, L.; Unger, E. L. Research Update: Recombination and Open-Circuit Voltage in Lead-Halide Perovskites. *APL Mater.* **2018**, *6*, 100702.
- (24) Stolterfoht, M.; Caprioglio, P.; Wolff, C. M.; Márquez, J. A.; Nordmann, J.; Zhang, S.; Rothhardt, D.; Hörmann, U.; Redinger, A.; Kegelmann, L.; et al. The Perovskite/Transport Layer Interfaces Dominate Non-Radiative Recombination in Efficient Perovskite Solar Cells. *arXiv Prepr. arXiv1810.01333* **2018**.
- (25) Staub, F.; Hebig, J.-C.; Mock, J.; Kirchartz, T.; Hempel, H.; Unold, T.; Rau, U.; Paetzold, U. W. Beyond Bulk Lifetimes: Insights into Lead Halide Perovskite Films from Time-Resolved Photoluminescence. *Phys. Rev. Appl.* **2016**, *6*, 1–13.
- (26) Abdi-Jalebi, M.; Andaji-Garmaroudi, Z.; Cacovich, S.; Stavrakas, C.; Philippe, B.; Richter, J. M.; Alsari, M.; Booker, E. P.; Hutter, E. M.; Pearson, A. J.; et al. Maximizing and Stabilizing Luminescence from Halide Perovskites with Potassium Passivation. *Nature* **2018**, *555*, 497–501.
- (27) Brenes, R.; Guo, D.; Osherov, A.; Noel, N. K.; Eames, C.; Hutter, E. M.; Pathak, S. K.; Niroui, F.; Friend, R. H.; Islam, M. S.; et al. Metal Halide Perovskite Polycrystalline Films Exhibiting Properties of Single Crystals. *Joule* **2017**, *1*, 155–167.
- (28) Momblona, C.; Gil-Escrig, L.; Bandiello, E.; Hutter, E. M.; Sessolo, M.; Lederer, K.; Blochwitz-Nimoth, J.; Bolink, H. J. Efficient Vacuum Deposited P-i-n and n-i-p Perovskite Solar Cells Employing Doped Charge Transport Layers. *Energy Environ. Sci.* **2016**, *9*, 3456–3463.
- (29) Hutter, E. M.; Eperon, G. E.; Stranks, S. D.; Savenije, T. J. Charge Carriers in Planar and Meso-Structured Organic-Inorganic Perovskites: Mobilities, Lifetimes, and Concentrations of Trap States. *J. Phys. Chem. Lett.* **2015**, *6*, 3082–3090.
- (30) Chandrashekar, S.; Abdi-Jalebi, M.; Sutton, R. J.; Hutter, E. M.; Savenije, T. J.; Stranks, S. D.; Snaith, H. J. Vapour-Deposited Cesium Lead Iodide Perovskites: Microsecond Charge Carrier Lifetimes and Enhanced Photovoltaic Performance. *ACS Energy Lett.* **2017**, *2*, 1901–1908.
- (31) Hutter, E. M.; Gélvez-Rueda, M. C.; Bartesaghi, D.; Grozema, F. C.; Savenije, T. J. Band-Like Charge Transport in Cs₂AgBiBr₆ and Mixed Antimony-Bismuth Cs₂AgBi_{1-x}Sb_xBr₆ Halide Double Perovskites. *ACS Omega* **2018**, *3*, 11655–11662.
- (32) Yang, J.-P.; Meissner, M.; Yamaguchi, T.; Zhang, X.-Y.; Ueba, T.; Cheng, L.-W.; Ideta, S.; Tanaka, K.; Zeng, X.-H.; Ueno, N.; et al. Band Dispersion and Hole Effective Mass of Methylammonium Lead Iodide Perovskite. *Sol. RRL* **2018**, *2*, 1800132.
- (33) Umari, P.; Mosconi, E.; De Angelis, F. Relativistic GW Calculations on CH₃NH₃PbI₃ and CH₃NH₃SnI₃ Perovskites for Solar Cell Applications. *Sci. Rep.* **2015**, *4*, 4467.

(34) Egger, D. A.; Bera, A.; Cahen, D.; Hodes, G.; Kirchartz, T.; Kronik, L.; Lovrincic, R.; Rappe, A. M.; Reichman, D. R.; Yaffe, O. What Remains Unexplained about the Properties of Halide Perovskites? *Adv. Mater.* **2018**, *30*, 1800691.

(35) Giorgi, G.; Fujisawa, J. I.; Segawa, H.; Yamashita, K. Small Photocurrent Effective Masses Featuring Ambipolar Transport in Methylammonium Lead Iodide Perovskite: A Density Functional Analysis. *J. Phys. Chem. Lett.* **2013**, *4*, 4213–4216.

(36) Quarti, C.; Mosconi, E.; De Angelis, F. Interplay of Orientational Order and Electronic Structure in Methylammonium Lead Iodide: Implications for Solar Cell Operation. *Chem. Mater.* **2014**, *26*, 6557–6569.

(37) Davies, C. L.; Filip, M. R.; Patel, J. B.; Crothers, T. W.; Verdi, C.; Wright, A. D.; Milot, R. L.; Giustino, F.; Johnston, M. B.; Herz, L. M. Bimolecular Recombination in Methylammonium Lead Triiodide Perovskite Is an Inverse Absorption Process. *Nat. Commun.* **2018**, *9*, 1–9.

(38) Brenner, T. M.; Egger, D. A.; Kronik, L.; Hodes, G.; Cahen, D. Hybrid Organic–Inorganic Perovskites: Low-Cost Semiconductors with Intriguing Charge-Transport Properties. *Nat. Rev. Mater.* **2016**, *1*, 16011.

(39) Hu, Y.; Hutter, E. M.; Rieder, P.; Grill, I.; Hanisch, J.; Aygüler, M. F.; Hufnagel, A. G.; Handloser, M.; Bein, T.; Hartschuh, A.; et al. Understanding the Role of Cesium and Rubidium Additives in Perovskite Solar Cells: Trap States, Charge Transport, and Recombination. *Adv. Energy Mater.* **2018**, *8*, 1703057.

(40) Ravishankar, S.; Gharibzadeh, S.; Roldán-Carmona, C.; Grancini, G.; Lee, Y.; Ralaiarisoa, M.; Asiri, A. M.; Koch, N.; Bisquert, J.; Nazeeruddin, M. K. Influence of Charge Transport Layers on Open-Circuit Voltage and Hysteresis in Perovskite Solar Cells. *Joule* **2018**, *2*, 788.

(41) Dänekamp, B.; Droseros, N.; Tsokkou, D.; Brehm, V.; Boix, P. P.; Sessolo, M.; Banerji, N.; Bolink, H. J. Influence of Hole Transport Material Ionization Energy on the Performance of Perovskite Solar Cells. *J. Mater. Chem. C* **2019**, *7*, 523–527.

(42) Abate, A.; Hagfeldt, A.; Gratzel, M.; Correa-Baena, J.-P.; Saliba, M.; Ummadisingu, A.; Seo, J.-Y.; Matsui, T.; Zakeeruddin, S. M.; Tress, W. R.; et al. Incorporation of Rubidium Cations into Perovskite Solar Cells Improves Photovoltaic Performance. *Science* **2016**, *354*, 206–209.

(43) Fu, R.; Zhao, Y.; Zhou, W.; Li, Q.; Zhao, Y.; Zhao, Q. Ultrahigh Open-Circuit Voltage for High Performance Mixed-Cation Perovskite Solar Cells Using Acetate Anions. *J. Mater. Chem. A* **2018**, *6*, 14387–14391.

(44) Zhang, W.; Pathak, S.; Sakai, N.; Stergiopoulos, T.; Nayak, P. K.; Noel, N. K.; Haghighirad, A. A.; Burlakov, V. M.; deQuilettes, D. W.; Sadhanala, A.; et al. Enhanced Optoelectronic Quality of Perovskite Thin Films with Hypophosphorous Acid for Planar Heterojunction Solar Cells. *Nat. Commun.* **2015**, *6*, 10030.

(45) Milot, R. L.; Eperon, G. E.; Snaith, H. J.; Johnston, M. B.; Herz, L. M. Temperature-Dependent Charge-Carrier Dynamics in $\text{CH}_3\text{NH}_3\text{PbI}_3$ Perovskite Thin Films. *Adv. Funct. Mater.* **2015**, *25*, 6218–6227.